ELSEVIER

Nuclear Instruments and Methods in Physics Research A 481 (2002) 696–707

NUCLEAR INSTRUMENTS & METHODS IN PHYSICS RESEARCH Section A

www.elsevier.com/locate/nima

Experimental verification of NOVICE transport code predictions of electron distributions from targets

S. Kronenberg[a,✠], G.J. Brucker[a,*], T. Jordan[a], E. Bechtel[a], F. Gentner[a], E. Groeber[b]

[a] *US Army, CECOM, Fort Monmouth, NJ, USA*

[b] *Project Manager, US Army NBC Defense Systems, RADIAC Project Office, Fort Monmouth NJ, USA*

Received 3 May 2001

Abstract

This paper reports the results of experiments that were designed to check the validity of the NOVICE Adjoint Monte Carlo Transport code in predicting emission-electron distributions from irradiated targets. Previous work demonstrated that the code accurately calculated total electron yields from irradiated targets. In this investigation, a gold target was irradiated by X-rays with effective quantum energies of 79, 127, 174, 216, and 250 keV. Spectra of electrons from the target were measured for an incident photon angle of 45°, an emission-electron polar angle of 45°, azimuthal angles of 0° and 180°, and in both the forward and backward directions. NOVICE was used to predict those electron-energy-distributions for the same set of experimental conditions. The agreement in shape of the theoretical and experimental distributions was good, whereas the absolute agreement in amplitude was within about a factor of 2 over most of the energy range of the spectra. Previous experimental and theoretical comparisons together with these results show that the code can be used to simulate the generation physics of those distributions.

1. Introduction and background

Previous publications [1–7] described the design and operating principle of gamma ray, directional sensors for locating and imaging sources of radiation. The Adjoint Monte Carlo NOVICE code [7] was used to simulate the responses of two types of sensors, namely, the Ionization Chamber and the Scintillation Detector [1,2]. The results of the simulations were in good agreement with the experimental measurements that involved detecting and locating sources of cesium-137 and cobalt-60 gamma rays and low energy X-rays in the energy range of 46–250 keV. Previous work demonstrated that the NOVICE code accurately predicted the total (i.e. forward + backward electrons) electron emissions from the high/low Z (atomic number) lead and lucite materials in those directional sensors. Another product of that study was a publication [8,9] of a monograph which contained NOVICE data for electron total yields from various irradiated target materials and thicknesses, photon energies, and incident photon angles. The data were in good agreement with

✠ Deceased during this investigation.

* Corresponding author. 18 Cheryl Drive, West Long Branch, NJ 07764, USA. Tel.: +1-732-427-5443; fax: +1-732-427-2667

0168-9002/02/$ - see front matter
PII: S0168-9002(01)01336-5

other experimental [10–12] and theoretical studies [13–15].

This study is a continuation of that earlier work which was expanded to investigate experimentally the details of the electron distributions in energy, polar angle, and azimuthal angle as well as calculations of those distributions by the NOVICE code. The results showed that the code's predictions were in good agreement with the shapes of the experimental energy distributions and in agreement with the absolute amplitudes within about a factor of 2 over most of the spectral energy range.

2. Experimental description

The radiation source that was used in the experiments is a Seifert ISOVOLT, X-ray machine capable of a maximum applied voltage of 300 KV and a tube current of 13–25 mA, depending on the voltage. The AC voltage is rectified and both current and voltage are very stable and accurately controlled. Table 1 lists the applied d.c. voltages, the filters used with each voltage, and the resulting effective energies (column 3 energies based on the differential in energy of the photon-dose-distribution, [16]). Those energies were determined by measuring the X-ray spectra with a sodium iodide spectrometer (Canberra model #35 Plus) for each combination of voltage and filter and then using the spectra to determine effective energies. The spectra were also used as the sources of radiation in the NOVICE code runs. Effective energies for these filter combinations that were determined by NIST (National Institute of Standards and Technology) are shown in column 4.

Table 1
X-ray generator applied voltages, filter combinations, and effective energies determined here and at NIST

Applied volts (KV)	Filter (mm)	Effective energy (keV)	Effective energy NIST (keV)
100	1.04Sn	79	85
150	4.13Sn	127	129
200	2.07Sn + 1.94Pb	174	178
250	2.07Sn + 3.88Pb	216	222
300	4.1Al + 3Sn + 5Pb	250	252

Fig. 1 is a diagram of the experimental setup. The X-ray collimator consisted of lead bricks 50.5 mm thick with a 15.9 mm diameter hole in the central brick which lined up with the center of the target. This aperture was large enough to flood the gold target, having a 6.35 mm diameter and a thickness of 0.2 mm. The target was located on a support of molybdenum wire with a 0.012 mm diameter. The gold target was made of 24 karat, 100% chemically pure gold.

Within the vacuum chamber (a converted, commercial pressure cooker), there were two more lead collimators, one at the point of X-ray penetration through the chamber wall and a second one on the far side of the chamber to catch and trap the uncollided photons. A cylindrical lead shield covered the detector and its output connection. This shield minimized the number of scattered electrons and photons that penetrated the side wall of the detector. In addition, the vacuum chamber and the region close to the exit port of the X-ray machine (such as the X-ray filter wheels) were covered by 3.18 mm thick lead sheet. The external lead shielding was used to decrease the scattered-photon background that existed around the vacuum chamber.

Both backgrounds, inside and outside the chamber, are not the usual cosmic ray background which is only about 10–15 μrad/h in our location. The X-ray generated level was about 200–500 mrad/h outside the chamber. An aluminum shield, 2.24 mm thick with a 7.14 mm diameter, was located close to the target so as to block electrons emitted from the target and to prevent them from reaching the detector. This arrangement allowed measurements of only the scattered X-rays and electrons. Thus, two types of spectra were measured, one produced by electrons from the target, scattered electrons, and scattered X-rays and the other by scattered electrons and photons that reached the detector and produced counts.

The target was oriented to provide an incident beam angle of 45° with the electron detector positioned at an angle of 45° relative to the plane of the target. This made the polar angle, $\varphi = 45^\circ$

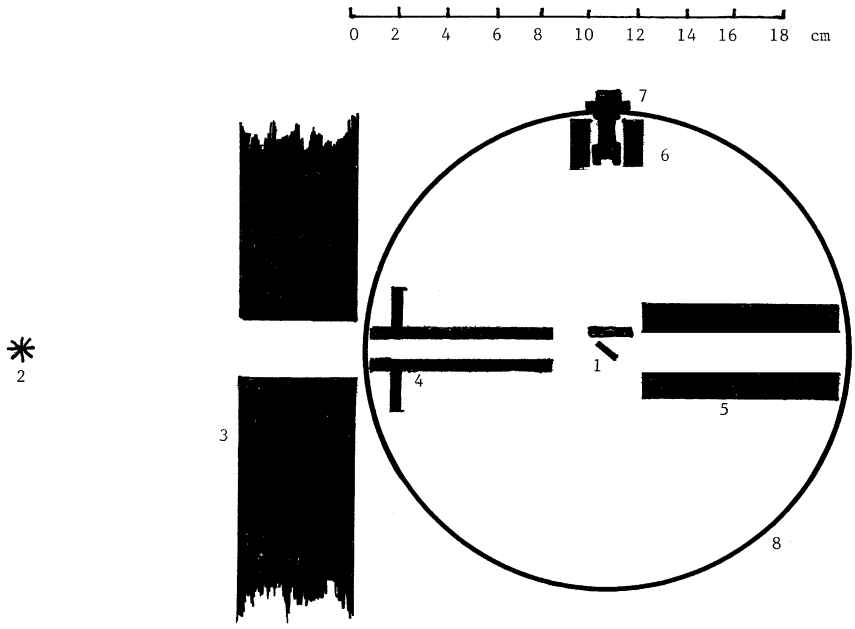

1. Target 6.4 mm diameter, Al Shield 7.14 mm diam
2. Xray source (50.4 cm from target).
3. Lead brick collimator
4. Collimator and shield (lead)
5. Black body (lead)
6. Detector Shield
7. PIPS solid state detector
8. Chamber (pressure cooker) with vacuum connections on top, wall thickness, 3.25 mm Al

Fig. 1. Drawing of experimental setup showing the vacuum chamber and the locations of the two lead collimators in the chamber and one outside, the target, aluminum shield, and the detector with its lead shield.

and the azimuthal angle, $\theta = 0^\circ$ for the electrons emitted in the forward direction. In the backward direction all of these angles were constant but the azimuthal angle was 180°. These three angles were used for all the experiments with the five X-ray quantum energies listed in Table 1. The orientation of the X-ray beam and detector remained fixed but the target was rotated by 90°. This rotation exposed the detector to the electrons emitted in either the forward or backward direction. The solid angle subtended by the detector, relative to the target, was 1.07×10^{-2} sr. Figs. 2a and b show diagrams of the coordinate system that was used in the experiment for both forward and backward directions of electron emission.

The detector is a solid state silicon PIPS (Passivated Implanted Planar Silicon) detector, (Canberra model #B50AM,) designed for beta measurements. Its depletion depth is 520 μm when fully depleted and its energy resolution is 6 keV. The electronic threshold is 18 keV and the active area is 50 mm^2. A Canberra preamplifier, #2001A and their Digital Spectrum Analyzer (DSA) 2000 spectrometer were used to process the detector signals. The digital electronic design of the threshold discriminator and amplifier in the DSA insures a very stable and reproducible system. The DSA was calibrated by exposing the detector to several different beta sources of radiation such as carbon-14 with a maximum beta energy of 158 keV, and technetium-99, 295 keV. The maximum electron energy of each source was used to determine the energy/channel-number conversion factor, 3.7 keV per channel-number.

3. Results

Fig. 3 shows the target electron + scatter electron + scatter X-ray spectrum, the scatter electron + scatter X-ray spectrum, and finally, the difference spectrum, corresponding to target electrons in

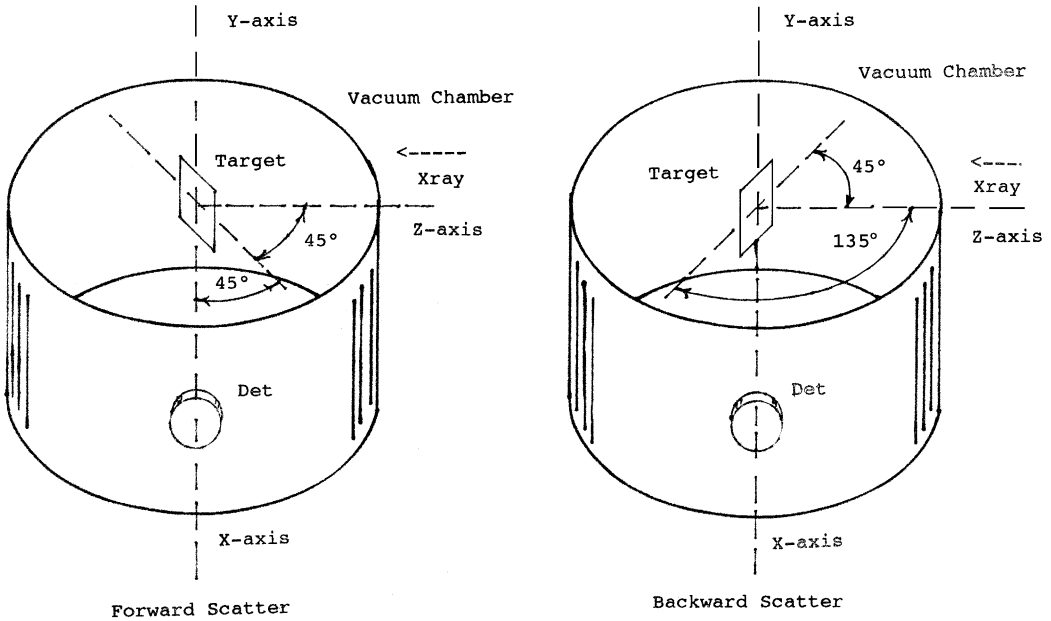

Fig. 2. a and b. Drawings of the coordinate system used in experiments for the forward and the backward electron emissions.

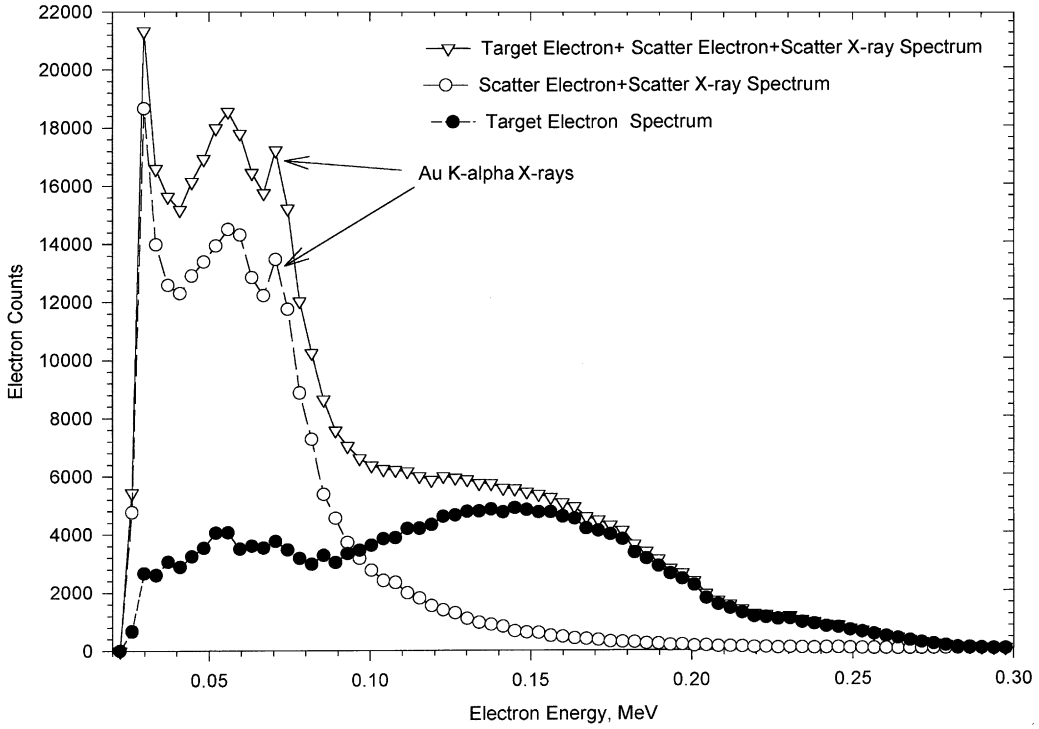

Fig. 3. Plots of unprocessed DSA-2000 forward emission data for the target electrons + scatter electrons + scatter X-rays, scatter electrons + scatter X-rays, and difference spectra obtained by irradiating the gold target, 0.2 mm thick, with 250 keV X-rays. Plots show the electron counts versus energy.

the backward direction. Those spectra were produced by 250 keV X-rays incident on the gold target and they are the unprocessed, experimental data. The number of electron counts at each energy (i.e. converting channel number to energy) are plotted versus the electron energy. For these specific spectra the counting time was 1800s.

Figs. 4–6 show the experimental and calculated electron energy distributions in the forward direction for 250, 216, and 174 keV X-rays on the gold target. Similarly, Figs. 7–9 compare the experimental and theoretical results for the backward direction and the same X-ray quanta. Figs. 10 and 11 compare the experimental and calculated results for 127 and 79 keV X-rays on the gold target with electron emission in the backward direction.

Fig. 12 demonstrates an application of the code to predicting the differential dose-distribution of electrons emitted from a tissue target 5 cm thick that is irradiated by monoenergetic photons of 6 and 15 MeV quantum energies. Data for two photon incident angles of 5.74° and 90°, relative to the plane of the target, are shown in the figure.

4. Discussion

The experimental, unprocessed, electron counts produced by X-ray photons of 250 keV incident on the gold target are shown in the spectra of Fig. 3 for the electrons emitted in the backward direction. One of the peaks in two of the spectra is produced by electrons with an energy of 70.7 keV. This peak response appears in all of the data for all photon energies equal to or greater than 127 keV on the gold target. We believe that the electrons at this energy of 70.7 keV are produced by the characteristic K-α_1 and α_2 photons at 69 and 67 keV [17], respectively, from the gold target. If lead was the source then we would have expected

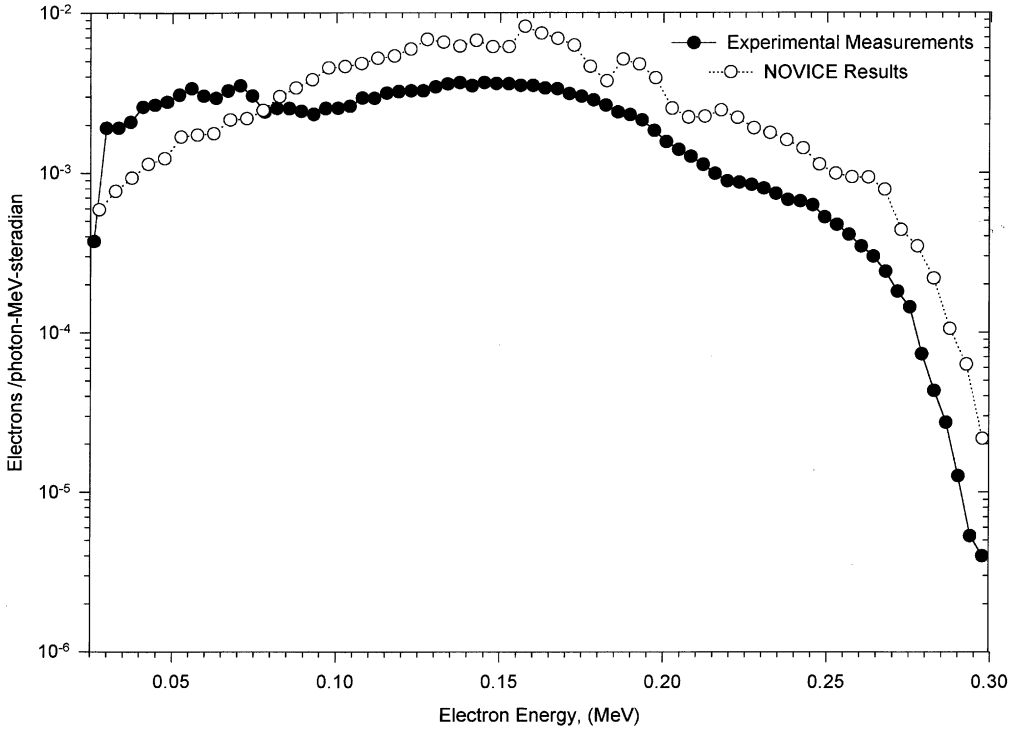

Fig. 4. Comparison of experimental and NOVICE calculated electron differential distributions from a gold target, 0.2 mm thick, irradiated by 250 keV X-rays at an incident angle of 45°. The electrons are emitted in the forward direction at a polar angle of 45° and an azimuthal angle of 0°. The experimental data points are the average values of five data sets.

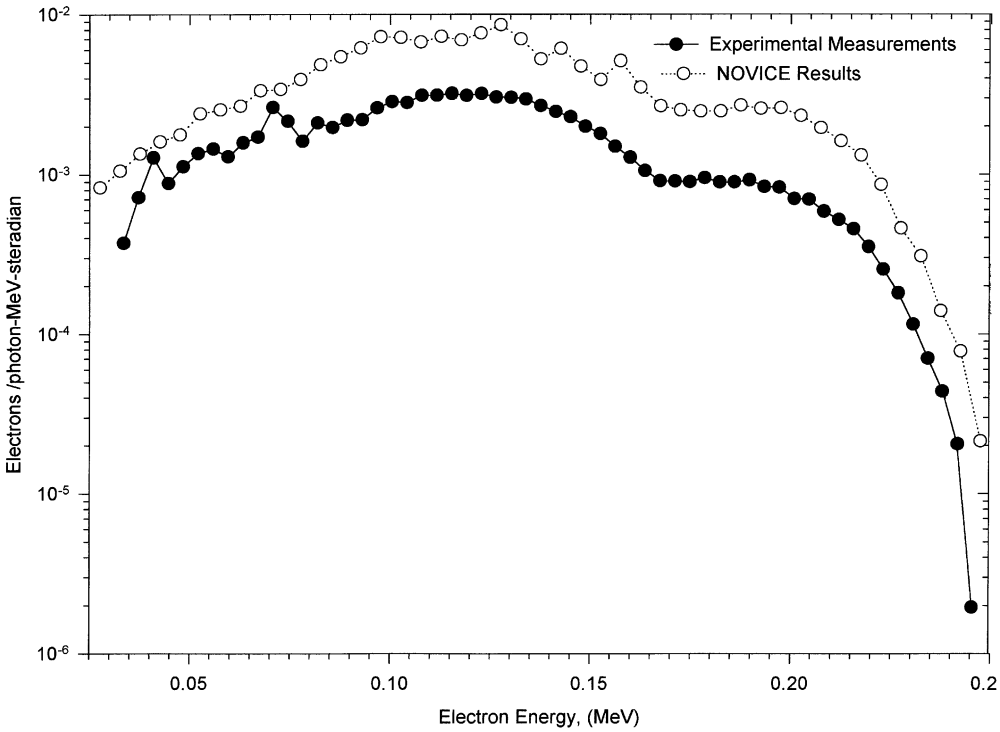

Fig. 5. Comparison of experimental and NOVICE calculated electron differential distributions from a gold target, 0.2 mm thick, irradiated by 216 keV X-rays at an incident angle of 45°. The electrons are emitted in the forward direction at a polar angle of 45° and an azimuthal angle of 0°.

an electron peak at about 73–82 keV. This peak disappeared when the gold target was removed and also when it was replaced by a tin or plastic-tissue target.

The spectrum produced when the target electrons were stopped by the aluminum shield is displayed by the open-circular symbols. This spectrum is the basic background spectrum which includes all the scattered photons from the aluminum chamber walls, scatter from the lead collimators, background photons external to the vacuum chamber, the characteristic gold photons, and scatter electrons. The detector converts all incident photons to electron pulses. Thus, the difference spectrum obtained by subtracting these two spectra yields the target electron spectrum, displayed by the plot of filled-circular symbols. For this photon energy and target material of high atomic number, photoelectric (about 76% of the total number of interactions, independent of angles) and Compton (about 15%) electrons were expected.

The difference distribution in Fig. 3 is the Compton distribution with a peak electron energy of about 130–150 keV. The expected Compton peak is about 124 keV for the effective X-ray energy of 250 keV. The theoretical distribution decreases in amplitude with decreasing electron energy from this peak value and then increases to its final peak value as the energy approaches zero. This distribution is superimposed on the background of scatter photoelectrons and photons. The width of the experimental X-ray spectrum for this effective energy of 250 keV is 182–298 keV, as measured at the zero base line.

Fig. 4 shows the comparison of experimental and NOVICE spectra obtained for the forward direction of electrons from the target and 250 keV X-rays. To establish an estimate of the

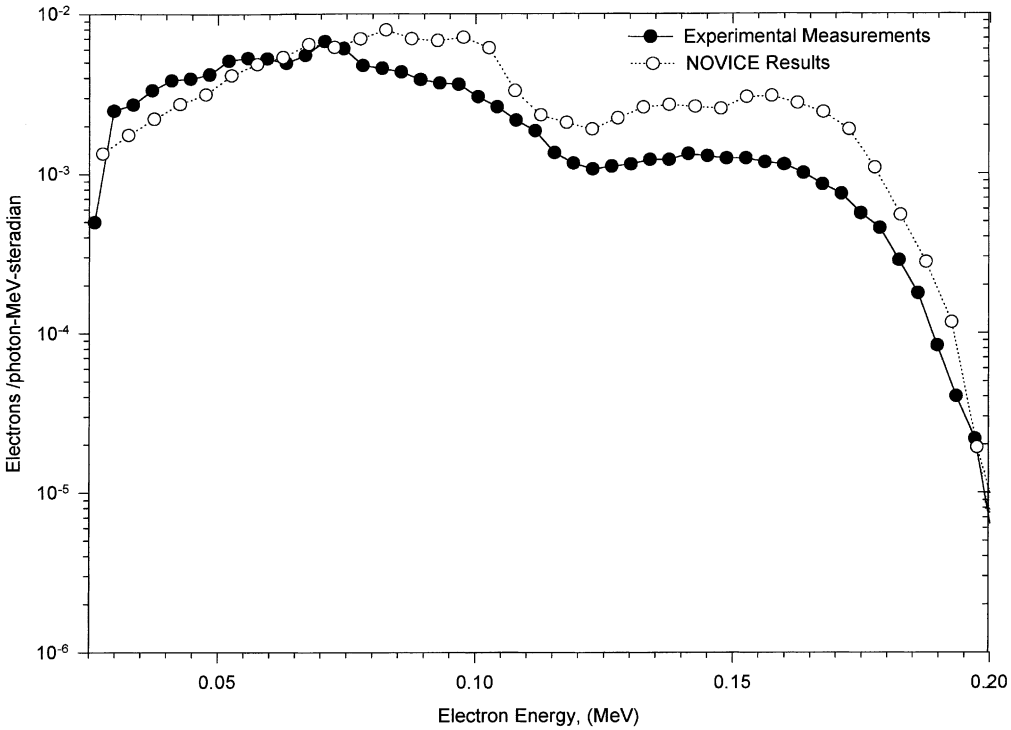

Fig. 6. Comparison of experimental and NOVICE calculated electron differential distributions from a gold target, 0.2 mm thick, irradiated by 174 keV X-rays at an incident angle of 45°. The electrons are emitted in the forward direction at a polar angle of 45° and an azimuthal angle of 0°.

reproducibility or uncertainty of the electron emission measurements, five independent measurements of the forward and backward data for an energy of 250 keV X-rays on the gold target were obtained. The protocol applied in taking these data was to measure the forward electron spectrum, then rotate the target and measure the backward spectrum. This procedure was used for all five sets of measurements which insured a worst case test of the reproducibility. The standard deviations for the five sets of measurements yielded an average deviation of $\pm 13\%$ for the total 75 data points per spectrum.

The experimental data are expressed in units of the number of electrons per photon, per MeV, and per steradian which are in the same units as in the NOVICE results. The number of incident photons on the target were determined by measuring the X-ray intensity at the target location using a Shonka–Wychoff spherical ionization chamber (Far West Technology, model IC17), 22.9 mm in diameter and measuring the ionization charge with a Keithley electrometer (model #614). The chamber's calibration is traceable back to NIST with an accuracy of $\pm 5\%$.

The solid angle subtended by the detector at the target in steradians was calculated from the measurements made within $\pm 1\%$. It can be seen from Fig. 4 that the agreement of theory and experiment in the distributions in shape is good over the spectral energy range. Most of the disagreement is in the absolute amplitudes of the calculated and measured spectra. The discrimator threshold of the spectrometer was set at 37 keV. We believe the low energy electrons near the threshold are probably due to the photons of characteristic radiation from gold and also the scatter photons.

The radiation model used in the NOVICE runs did not include those photon effects. The number

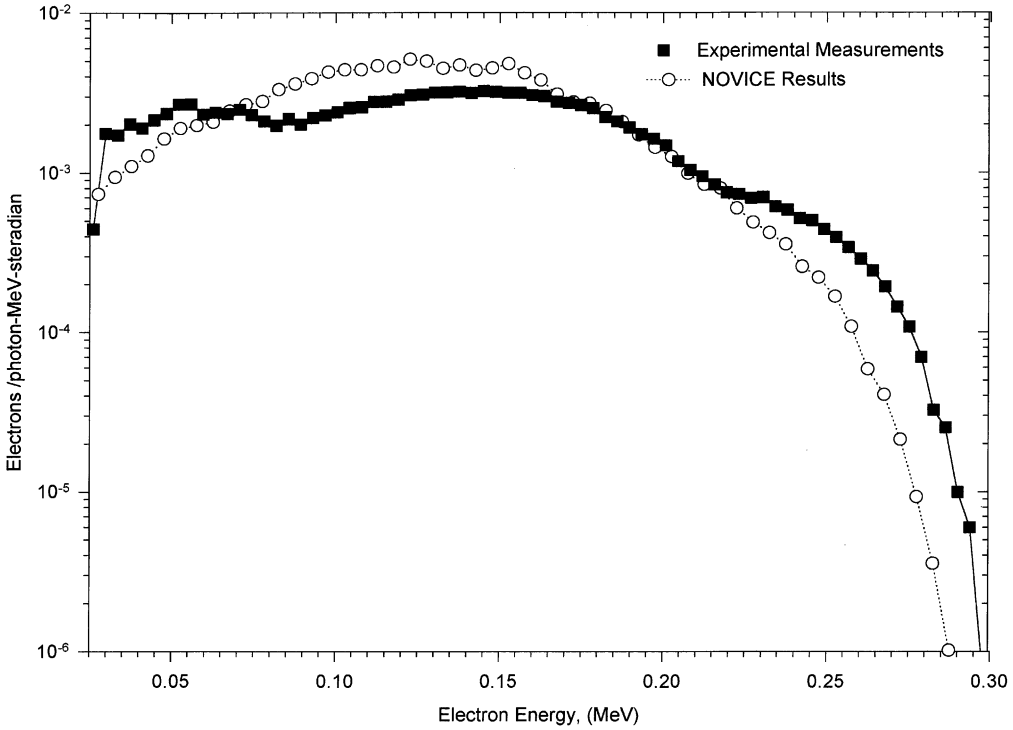

Fig. 7. Comparison of experimental and NOVICE calculated electron differential distributions from a gold target, 0.2 mm thick, irradiated by 250 keV X-rays at an incident angle of 45°. The electrons are emitted in the backward direction at a polar angle of 45° and an azimuthal angle of 180°.

of electron histories achieved in a NOVICE run was set at 5×10^5. This value produced a statistical error of 2–4% for 60 data points of energy, covering a range from 0.2 to 300 keV. The largest error in the calculations was probably the measured X-ray spectra. However, prior to these spectral measurements, the effective energies for the same filter combinations were determined by NIST. Those effective energies specified by NIST for the filters are listed in the last column of Table 1. The difference in the two values of effective energies range from 2% to 7%. Thus, the accuracy of the X-ray spectra is about 10% relative to the NIST values that were determined when the filters were initially characterized. The agreement in amplitude as well as shape in the data is strong support for the validity of the NOVICE code.

Figs. 5 and 6 show a comparison of experimental data and NOVICE calculations for X-ray quantum energies of 216 and 174 keV and for the forward direction of electron emission. It can be seen that the agreement of the experimental and theoretical distributions is about the same as for the 250 keV X-rays. Figs. 7–9 show the comparisons for the same energy ranges but now for the backward direction. The agreement in the measured and theoretical amplitudes is slightly better for the 250 keV results in the backward direction as compared to the forward emissions. The similarity in shape of the backward and forward emissions is good for the same energies of 250, 216, and 174 keV.

Confirmation of experimental data by theoretical electron spectra for incident X-ray energies of 127 and 79 keV was about the same as for the higher energies. Figs. 10 and 11 show the comparisons of measurements and calculations for these two energies in the backward direction. For these lower energies, the errors increase due to the poorer energy resolution of the detector. The

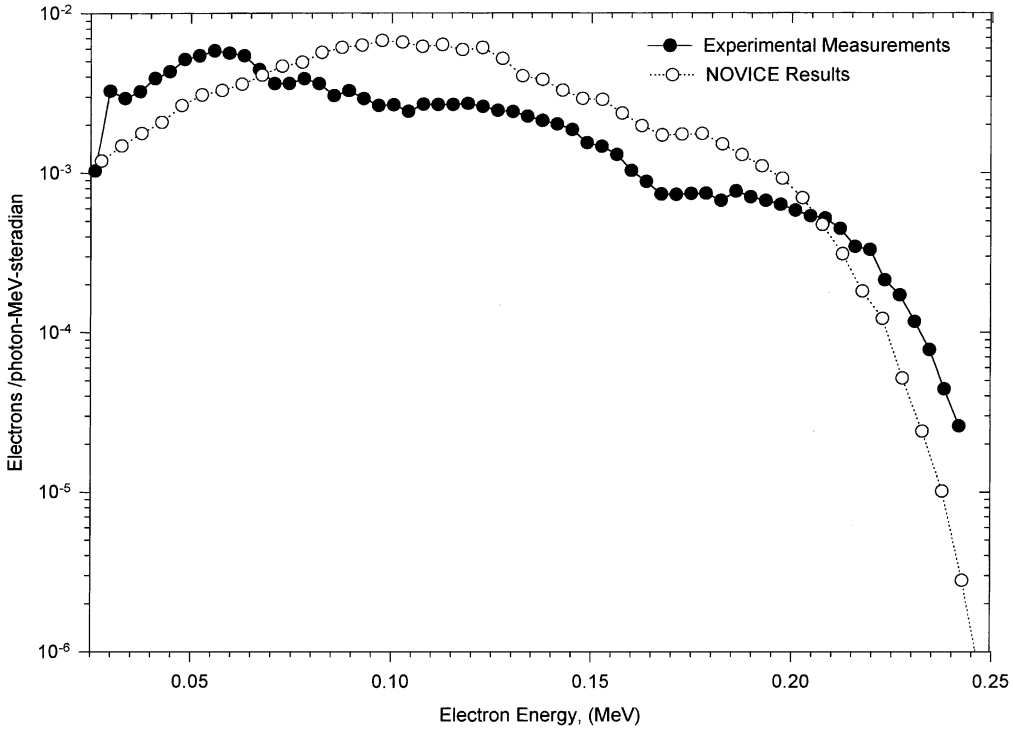

Fig. 8. Comparison of experimental and NOVICE calculated electron differential distributions from a gold target, 0.2 mm thick, irradiated by 216 keV X-rays at an incident angle of 45°. The electrons are emitted in the backward direction at a polar angle of 45° and an azimuthal angle of 180°.

scatter contributions from lower energy electrons also increase.

The similarity in the absolute amplitudes and shapes of the theoretical and experimental distributions in both forward and backward directions for this range of X-ray energies support the potential use of the NOVICE code in medical therapy applications. The differential energy, polar, and azimuthal electron distributions can be converted to differential dose-distributions [5]. Fig. 12 shows a plot of an angular, differential, dose-distribution for a 5 cm thick tissue target irradiated by photons of 6 and 15 MeV quantum energies. The photon incident angles are 5.74° and 90° (measured relative to the target plane) and the polar angle of the electrons from the target is 45° with integration over azimuthal angles from 0° to 180°. For the 90° angle of incidence (photons normal to the target plane), the azimuthal contribution to the distribution is constant throughout this angular range. One million histories were specified in obtaining the data in Fig. 12. It can be seen that the statistical errors of data points are still significant for the higher energy electrons in the range of 11–15 MeV.

The target model used in the code's calculations was a 3-dimensional one with x- and y-coordinates equal to 1 m. These latter calculations simulate approximately a cancer treatment, using a LINAC machine providing bremsstrahlung spectra, generated by 6 and 15 MeV electrons. Future studies will use the actual filtered spectra and a model of a man as inputs to NOVICE runs. In addition, the primary and scattered photons will be tracked as well as the electrons generated along the photon paths. The plots illustrate the dependence of dose on photon quantum energy and angle of incidence. It is interesting to note that the shallow angle (i.e. 5.74°) maximum doses are only about a factor of 3.5 smaller than the 90° values for the 15 MeV

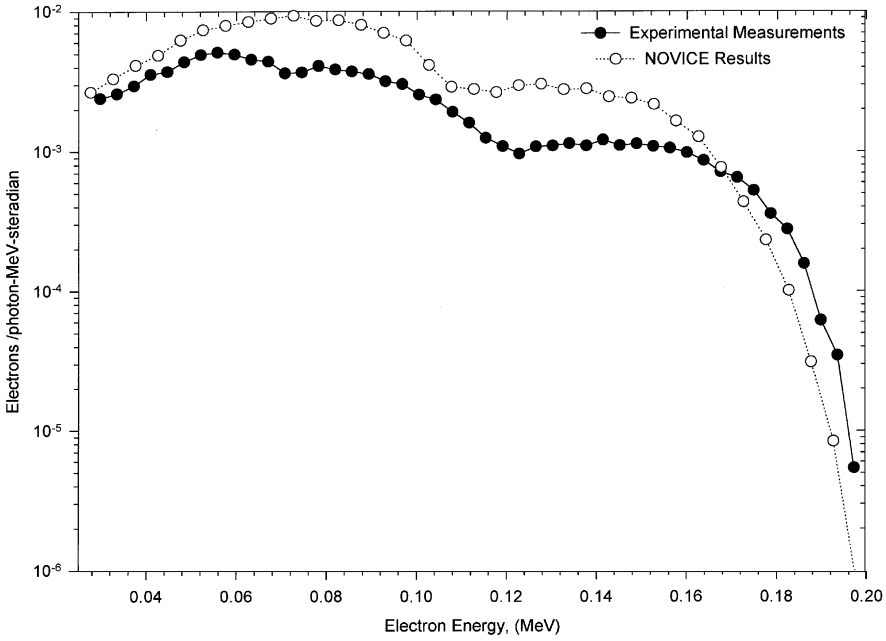

Fig. 9. Comparison of experimental and NOVICE calculated electron differential distributions from a gold target, 0.2 mm thick, irradiated by 174 keV X-rays at an incident angle of 45°. The electrons are emitted in the backward direction at a polar angle of 45° and an azimuthal angle of 180°.

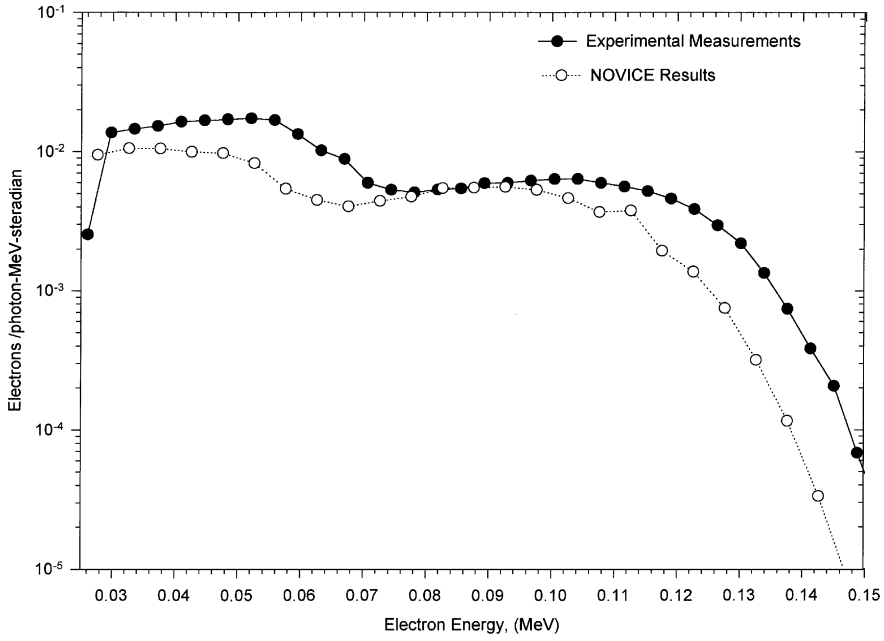

Fig. 10. Comparison of experimental and NOVICE calculated electron differential distributions from a gold target, 0.2 mm thick, irradiated by 127 keV X-rays at an incident angle of 45°. The electrons are emitted in the backward direction at a polar angle of 45° and an azimuthal angle of 180°.

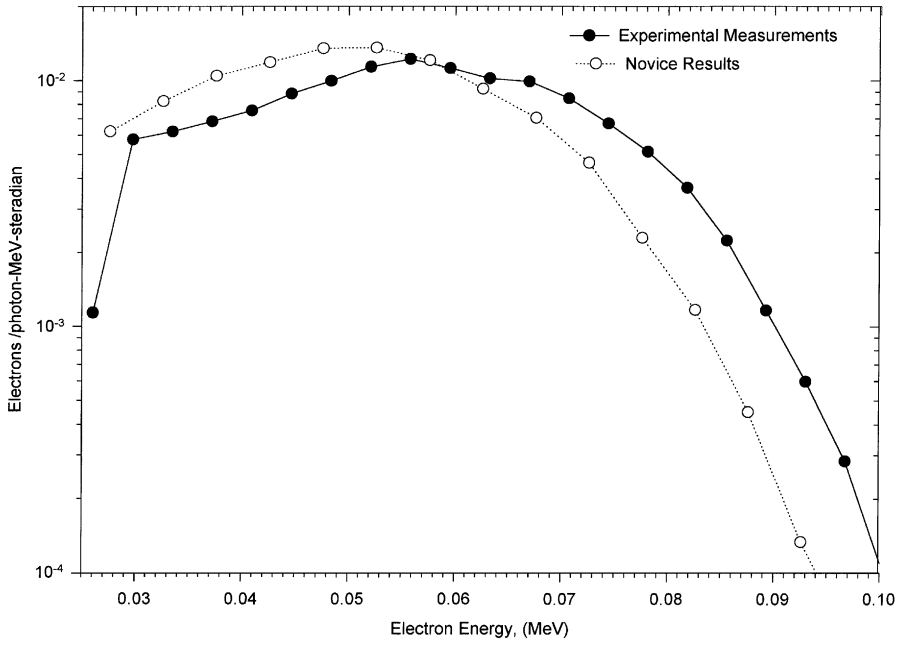

Fig. 11. Comparison of experimental and NOVICE calculated electron differential distributions from a gold target, 0.2 mm thick, irradiated by 79 keV X-rays at an incident angle of 45°. The electrons are emitted in the backward direction at a polar angle of 45° and an azimuthal angle of 180°.

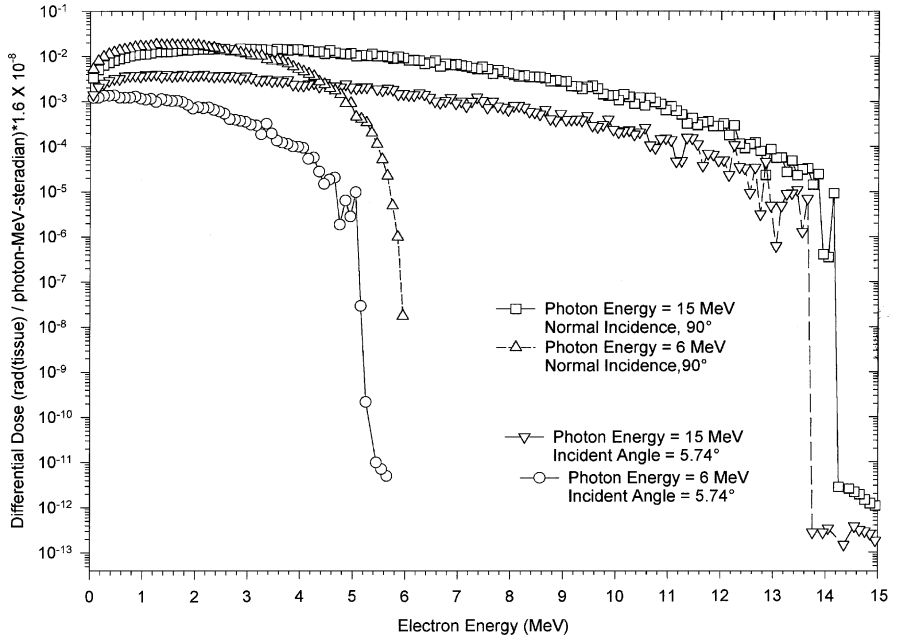

Fig. 12. This figure shows the calculated angular, differential dose-distribution for 6 and 15 MeV photon quantum energies, incident on a tissue target 5 cm thick, versus electron energy. The data are for photon-incident angles of 5.74° and 90° relative to the target plane, polar angle = 45, and integrated over azimuthal angles.

photons. This suggests that the scatter photons from the primary target that are incident at shallow and larger angles on surrounding secondary targets (e.g. other tissue and organs) can produce high doses. In the case of the lower energy of 6 MeV, the difference in the comparison of the results for the two angles of incidence is larger, that is a factor of about 15. It can be seen that most of the electron dose is due to the low energy electrons in the range of 0–3 and 0–10 MeV for the 6 and 15 MeV photons, respectively.

5. Conclusions

It can be concluded from the agreement of the experimental electron distributions in both forward and backward directions with the NOVICE calculations that this transport code predicts the emission-electron-distributions in energy, polar angle, and azimuthal angle for an incident photon angle of 45° on a gold target and X-ray quantum energies in the range of 79–250 keV.

Experimental verification of the code's calculations of total electron yield [6,10], and this study's results justify the application of the code to calculating 3-dimensional dose-distributions for cancer treatments. Those distributions for the tumors themselves as well as the nearby healthy tissues and organs would be available for investigation.

References

[1] S. Kronenberg, G.J. Brucker, E. Bechtel, F. Gentner, Directional detector for arrays of gamma ray and X-ray sources, Nucl. Instr. and Meth. A 378 (1996) 531–540.

[2] S. Kronenberg, G.J. Brucker, E. Bechtel, F. Gentner, A. Lee, Locating and imaging sources of gamma and X-radiation directly or through thick shields, Nucl. Instr. and Meth. A 387 (1997) 401–409.

[3] S. Kronenberg, G.J. Brucker, High angular resolution sensing of gamma rays in space, Opt. Soc. Eng. Instrum., (SPIE) Conf. J. 3116 (1997) 49–56.

[4] S. Kronenberg, G.J. Brucker, E. Bechtel, Solid state sensor for locating and imaging sources of gamma and X-radiation, IEEE Trans. Nucl. Sci. NS-45(3) (1998) 1481.

[5] S. Kronenberg, G.J. Brucker, E. Bechtel, The concept of the angular differential dose of ionizing radiation and its measurement, J. Appl. Radiat. Isot. 48 (9) (1997) 1251–1256.

[6] S. Kronenberg, G.J. Brucker, T. Jordan, NOVICE 3-d transport code simulation of directional photon sensors, Nucl. Instr. and Meth. A 413 (1998) 263–274.

[7] T. Jordan, NOVICE: A radiation transport/shielding code, Experimental and Mathematical Consultants, report #EMP.L82.001, 1982.

[8] S. Kronenberg, G.J. Brucker, T. Jordan, Electron yields from irradiated targets versus photon incident angle and quantum energy, Radiat. Phys. Chem. 56 (1999) 267–280.

[9] S. Kronenberg, G.J. Brucker, T. Jordan, Monograph on Electron Yields from Irradiated Targets versus Photon Incident Angle and Quantum Energy. The US Government Printing Office, New York City, N.Y., April, 1999.

[10] M.Ya. Grudskii, N.N. Roldugin, V.V. Smirnov, A.F. Adadurov, V.T. Lazurik, Experimental investigation and Monte Carlo calculation of photon-induced electron emission from solids, Nucl. Instr. and Meth. 227 (1984) 126–134.

[11] E.A. Burke, J.A. Wall, A.R. Frederickson, Radiation-Induced low energy electron emission from metals, IEEE Trans. Nucl. Sci. NS-17 (1970) 193–199.

[12] A.R. Frederickson, E.A. Burke, Total electron backscatter and backemission yields from metals bombarded at several angles by 0.4 to 1.4 MeV electrons, IEEE Trans. Nucl. Sci. NS-19 (1972) 160–166.

[13] T.A. Dellin, R.E. Huddleston, C.J. MacCallum, Second generation analytical photo-Compton current methods, IEEE Trans. Nucl. Sci. NS-22 (1975) 2549–2555.

[14] J.A. Halbleib, R.P. Kensek, G.D. Valdez, S.M. Seltzer, M.J. Berger, ITS: the integrated TIGER series of electron/photon transport codes-version 3.0, IEEE Trans. Nucl. Sci. NS-39 (1992) 1025–1030.

[15] L.J. Lorence, R.P. Kensek, J.A. Halbleib, J.E. Morel, Adjoint electron-photon transport Monte Carlo calculations with ITS, IEEE Trans Nucl. Sci. NS-42 (1995) 1895–1901.

[16] W.J. Iles, The computation of bremsstralung X-ray spectra over an energy range 15 keV to 300 keV, National Radiological Protection Board, NRPB-R204, Chilton, Didcot, Oxon OX 11 ORQ, 1987.

[17] R.C. Wesst (Ed.), Handbook of Chemistry and Physics, 60th Edition, CRC Press, Boca Raton, FL, 1979.